Article

Cell Reports

Dendrite-Specific Amplification of Weak Synaptic Input during Network Activity *In Vivo*

Graphical Abstract

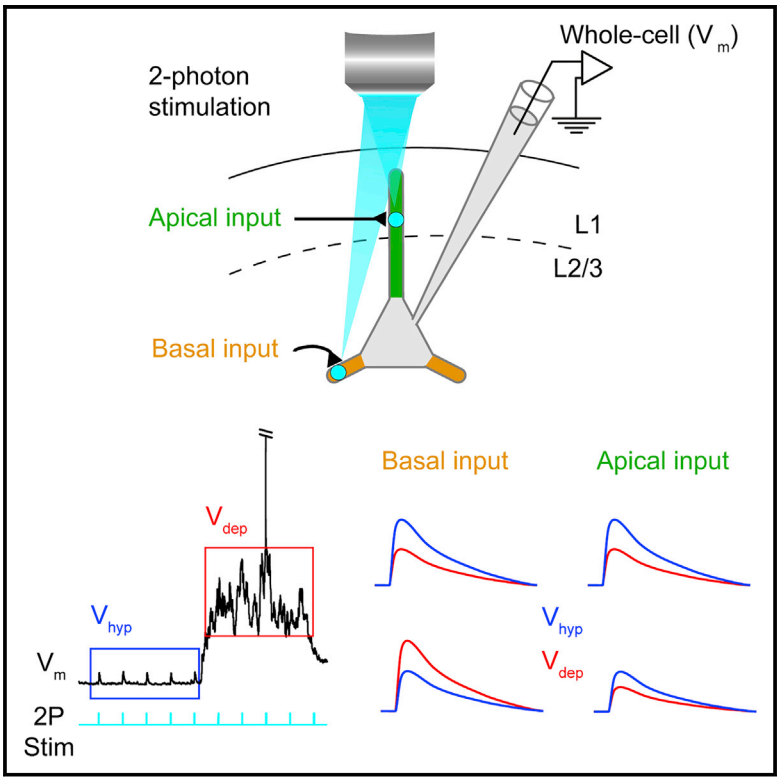

Authors

Leiron Ferrarese, Jean-Sébastien Jouhanneau, Michiel W.H. Remme, ..., Balázs Rózsa, Susanne Schreiber, James F.A. Poulet

Correspondence

james.poulet@mdc-berlin.de

In Brief

Ferrarese et al. investigate the impact of network activity on synaptic integration in cortical L2/3 pyramidal neurons *in vivo*. They report a reduction of apical dendritic inputs but an amplification of small-amplitude basal inputs during depolarized phases of slow network activity. The amplification is dependent on postsynaptic voltage-gated channels.

Highlights

- *In vivo* subcellular optogenetic stimulation of cortical layer 2/3 pyramidal neurons
- Slow network activity amplifies small-amplitude basal dendritic inputs
- Apical inputs are reduced during depolarized phases of slow network activity
- Basal input amplification is mediated by postsynaptic voltage-gated channels

Ferrarese et al., 2018, Cell Reports *24*, 3455–3465
September 25, 2018 © 2018 The Authors.
https://doi.org/10.1016/j.celrep.2018.08.088

CellPress

Cell Reports
Article

OPEN ACCESS
CellPress

Dendrite-Specific Amplification of Weak Synaptic Input during Network Activity *In Vivo*

Leiron Ferrarese,[1,2,7] Jean-Sébastien Jouhanneau,[1,2,7] Michiel W.H. Remme,[3] Jens Kremkow,[1,2,3] Gergely Katona,[4,5] Balázs Rózsa,[4,6] Susanne Schreiber,[3] and James F.A. Poulet[1,2,8,*]

[1]Department of Neuroscience, Max Delbrück Center for Molecular Medicine in the Helmholtz Association (MDC), Berlin-Buch, Robert-Rössle-Str. 10, 13092 Berlin, Germany
[2]Neuroscience Research Center and Cluster of Excellence NeuroCure, Charité-Universitätsmedizin Berlin, Charitéplatz 1, 10117 Berlin, Germany
[3]Department of Biology, Institute for Theoretical Biology, Humboldt-Universität zu Berlin and Bernstein Center for Computational Neuroscience Berlin, Philippstrasse 13, 10115 Berlin, Germany
[4]Laboratory of 3D Functional Network and Dendritic Imaging, Institute of Experimental Medicine, Hungarian Academy of Sciences, Budapest 1083, Hungary
[5]MTA-PPKE ITK-NAP B – 2p Measurement Technology Group, The Faculty of Information Technology, Pázmány Péter Catholic University, Budapest 1083, Hungary
[6]The Faculty of Information Technology, Pázmány Péter Catholic University, Budapest 1083, Hungary
[7]These authors contributed equally
[8]Lead Contact
*Correspondence: james.poulet@mdc-berlin.de
https://doi.org/10.1016/j.celrep.2018.08.088

SUMMARY

Excitatory synaptic input reaches the soma of a cortical excitatory pyramidal neuron via anatomically segregated apical and basal dendrites. *In vivo*, dendritic inputs are integrated during depolarized network activity, but how network activity affects apical and basal inputs is not understood. Using subcellular two-photon stimulation of Channelrhodopsin2-expressing layer 2/3 pyramidal neurons in somatosensory cortex, nucleus-specific thalamic optogenetic stimulation, and paired recordings, we show that slow, depolarized network activity amplifies small-amplitude synaptic inputs targeted to basal dendrites but reduces the amplitude of all inputs from apical dendrites and the cell soma. Intracellular pharmacology and mathematical modeling suggests that the amplification of weak basal inputs is mediated by postsynaptic voltage-gated channels. Thus, network activity dynamically reconfigures the relative somatic contribution of apical and basal inputs and could act to enhance the detectability of weak synaptic inputs.

INTRODUCTION

A defining feature of cortical pyramidal neurons is their two major classes of dendrites. Thin basal dendrites extend horizontally from the soma and a thicker apical trunk dendrite projects toward the pial surface, extending thinner oblique branches. The integration of synaptic inputs from apical and basal dendrites lies at the heart of single-cell computation (Magee, 2000; Spruston, 2008), but little is known about this process *in vivo*.

Recent work has suggested that synaptic inputs to basal and apical dendrites of pyramidal neurons in cortical layers 2/3 and 5 are functionally distinct. GABA-ergic inhibitory somatostatin-expressing neurons, for example, are thought to target apical dendrites while parvalbumin-expressing GABA-ergic neurons more strongly innervate somato-basal regions (Jiang et al., 2013; Markram et al., 2004). Anatomical and mapping studies suggest that different sources of excitatory input are also anatomically segregated. Apical dendrites may receive excitatory thalamic input from higher order thalamic nuclei (e.g., the posteromedial nucleus [POm]) and distant cortical regions (Meyer et al., 2010; Petreanu et al., 2009; Veinante and Deschênes, 2003), whereas basal dendrites receive input from neighboring cortical neurons (Feldmeyer et al., 2006) and sensory-driven input either directly from the primary lemniscal ventral posteromedial nucleus (VPM) (Meyer et al., 2010; Petreanu et al., 2009) or indirectly via layer 4 neurons (Feldmeyer et al., 2002). Here, we investigated whether excitatory inputs to apical and basal dendrites are treated differently during synaptic integration in single layer 2/3 pyramidal neurons *in vivo*.

In vivo and *in vitro* measurements have shown that the vast majority of unitary excitatory postsynaptic potentials ($_u$EPSPs) reaching the soma of a pyramidal neuron via apical and basal dendrites are small in amplitude (<1 mV) (Bruno and Sakmann, 2006; Feldmeyer et al., 2006; Jouhanneau et al., 2015, 2018; Lefort et al., 2009; Markram et al., 1997; Song et al., 2005). Their small size is in part due to the high axial resistance of thin dendrites that impose strong cable filtering, a feature that is especially evident in the thin basal dendrites (Nevian et al., 2007; Williams and Stuart, 2002). Moreover, *in vivo*, cortical neurons generate action potentials and perform synaptic integration during depolarized phases of spontaneous synaptic activity (Chen et al., 2013; Cowan and Wilson, 1994; Petersen et al., 2003; Steriade et al., 1993) that could alter synaptic transmission via activation of voltage-gated ion channels, a change in the glutamatergic driving force, and an increase in background conductance. *In vivo* data comparing EPSPs during synaptically quiescent, hyperpolarized downstate with active, depolarized upstate

This is an open access article under the CC BY-NC-ND license (http://creativecommons.org/licenses/by-nc-nd/4.0/).

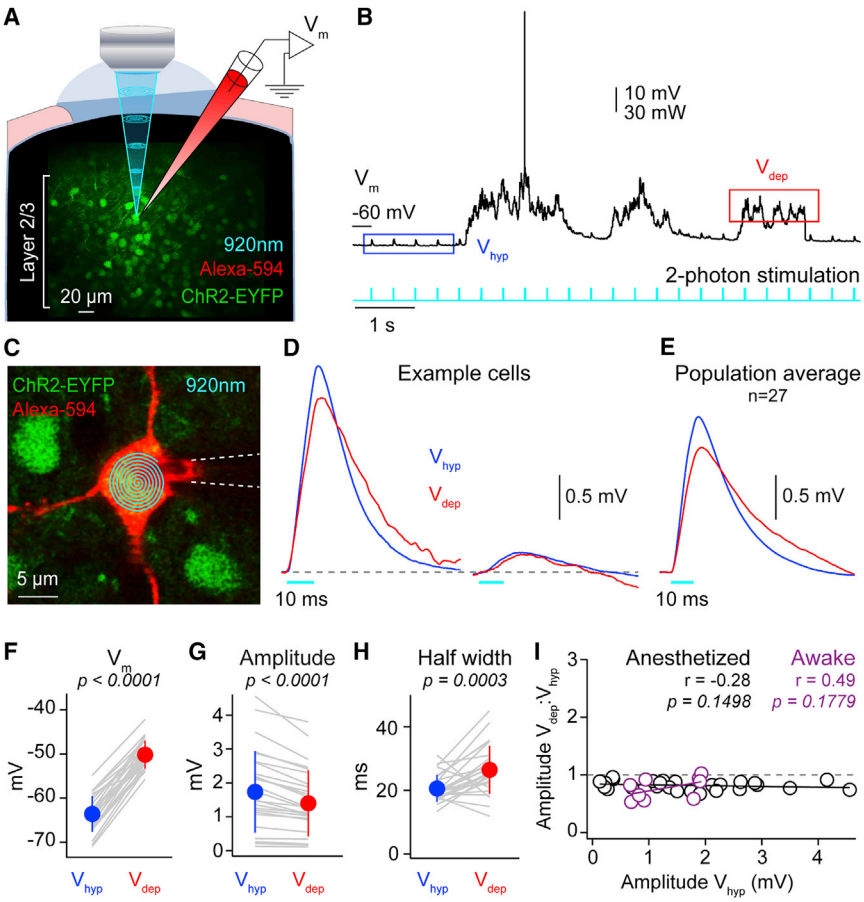

Figure 1. Response to Somatic Two-Photon Stimulation of ChR2-Expressing Layer 2/3 Pyramidal Neurons Is Reduced in Amplitude during Depolarized Phases of Slow Network Activity

(A) Schematic showing two-photon laser stimulation of ChR2-EYFP-expressing neurons.

(B) Example somatic membrane potential (V_m) recording of a layer 2/3 cortical pyramidal neuron under urethane anesthesia showing small depolarizations (optogenetic potentials [OPs]) in response to two-photon laser stimulation (cyan) during hyperpolarized (V_{hyp}, blue) and depolarized (V_{dep}, red) periods of network activity.

(C) Example *in vivo* image showing the path of the somatic laser stimulation (cyan).

(D) Overlaid, mean light-evoked OPs to somatic stimulation (OP_{som}, cyan) during V_{hyp} (blue) and V_{dep} (red) from two example neurons with different response amplitudes.

(E) Same as (C) but for population average.

(F) Somatic V_m increase as neurons transition from V_{hyp} to V_{dep}. Gray lines show data from individual cells, filled circles with error bars the mean ± SD.

(G) OP_{som} amplitude is significantly lower during V_{dep} than V_{hyp}.

(H) OP_{som} half width is significantly longer during V_{dep} than V_{hyp}.

(I) No significant correlation between the ratio V_{dep}:V_{hyp} OP_{som} amplitude and the $\log_{10}$ of V_{hyp} OP_{som} amplitude in awake (purple) and anesthetized (black). Black and purple lines are linear fits.

phases of spontaneous activity have shown mixed results with a reduction (Bruno and Sakmann, 2006; Crochet et al., 2005), no change (Pala and Petersen, 2015), and a rescaling (Reig et al., 2015) of amplitude. The reason for these differences is unclear, but one possibility is that the modulation of synaptic input amplitude during network activity is determined by the input location.

To address this hypothesis, we used direct dendritic stimulation and paired recordings to evoke weak subthreshold inputs to apical and basal dendrites of layer 2/3 pyramidal neurons during different phases of network activity *in vivo*. Unexpectedly, we found that depolarized phases of slow network activity amplified weak EPSPs originating from basal dendrites while reducing the amplitude of all somatic and apical inputs. Intracellular pharmacology and modeling suggest that basal input amplification relies on postsynaptic voltage-gated channels.

RESULTS

Mimicking Synaptic Inputs to Layer 2/3 Pyramidal Neurons with Subcellular Two-Photon Optogenetic Stimulation *In Vivo*

To mimic synaptic inputs from basal and apical branches within a physiologically relevant range (0.04–4.6 mV), we optically stimulated the soma or single dendritic branches of channelrhodopsin2 (ChR2)-expressing neurons *in vivo* and monitored the input with somatic whole-cell recordings. We expressed hChR2(T159C)-p2A-EYFP in layer 2/3 excitatory pyramidal neurons using a viral vector (AAV2/9) and the αCamKII promoter. Three to five weeks later, we performed somatic two-photon targeted whole-cell patch-clamp recordings of ChR2-EYFP-expressing neurons (Figures 1A–1C) in urethane anesthetized or awake mice during slow (<6-Hz) network activity. Visually targeted recordings were established from pyramidal neurons at a depth of 110.3 ± 22.2 μm (n = 158), using whole-cell pipettes filled with intracellular solution and Alexa Fluor 594. The mean membrane potential (V_m) in anesthetized mice was −57.96 ± 5.55 mV (n = 138) but oscillated between hyperpolarized (V_{hyp}) and depolarized (V_{dep}) phases (Figure 1B). Following establishment of the whole-cell configuration, the intracellular Alexa Fluor 594 dye was used to target two-photon optogenetic stimulation to either the soma or basal or apical oblique dendrites 17–135 μm from the soma.

We first stimulated the soma with 10 ms, 3 Hz spiral-patterned two-photon laser stimulation (Figure 1C). This reliably triggered depolarizing optogenetic potentials (OPs) with an onset latency during V_{hyp} of 0.69 ± 0.22 ms, indicating a direct response to the optical stimulation, a rise time of 5.22 ± 0.93 ms, peak time of 12.54 ± 1.8 ms, half-width of 20.55 ± 4.25 ms, and decay time of 20.97 ± 9.07 ms (n = 27 cells). OPs were not present when stimulating wild-type neurons or neurons expressing

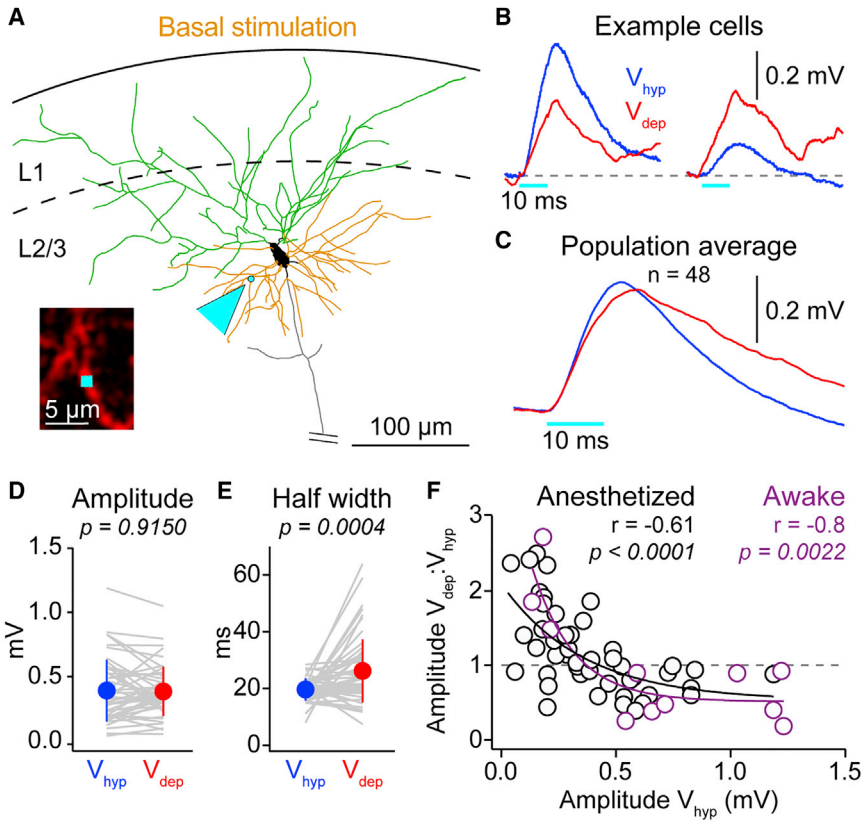

Figure 2. Amplification of Weak Optogenetically Evoked Inputs from Basal Dendrites of Layer 2/3 Pyramidal Neurons during Depolarized Phases of Slow Network Activity

(A) Reconstruction of example layer 2/3 pyramidal neuron showing the soma (black), apical dendrites (green), and basal dendrites (orange), with the basal dendrite two-photon stimulation site highlighted by cyan arrowhead. Inset shows *in vivo* image of Alexa-Fluor-594-filled dendrite in red and optogenetic stimulation site in cyan.

(B) Overlaid mean OP_{bas} from 2 example cells show a (left) decreased and (right) increased response during V_{dep}.

(C) Population average OP_{bas} from V_{hyp} and V_{dep}.

(D) Amplitude of OP_{bas} in V_{dep} and V_{hyp} is not significantly different. Gray lines show data from individual cells, filled circles with error bars the mean ± SD.

(E) OP_{bas} half-width is significantly longer during V_{dep} than V_{hyp}.

(F) A negative correlation between the ratio of the OP_{bas} amplitude in V_{dep}:V_{hyp} and V_{hyp} OP_{bas} amplitude in awake (purple) and anesthetized (black) mice results in smaller amplitude inputs increasing and larger amplitude inputs decreasing in amplitude during V_{dep}. Correlations performed on the V_{dep}:V_{hyp} amplitude and $\log_{10}$ of the V_{hyp} OP_{bas} amplitude are shown. Black and purple lines are single exponential fits.

EYFP, but not ChR2, and were dependent on accurate subcellular targeting (Figure S1). 10 ms two-photon laser stimuli were delivered at 3 Hz, because this was the highest frequency not susceptible to adaptation (Figures 1B and S1C–S1G). To stimulate dendrites, a small square of two-photon laser stimulation (1 μm^2) was directed to individual branches (Figures 2A and S1L–S1S). Stimulation of apical and basal dendrites in V_{hyp} evoked an OP with similar kinetics (apical: latency 1.79 ± 0.64 ms, rise time 6.35 ± 1.97 ms, peak time 15.01 ± 3.03 ms, half width 22.32 ± 6.53 ms, decay time 27.96 ± 18.06 ms, n = 37; basal: latency 1.58 ± 0.67 ms, rise time 5.32 ± 0.83 ms, peak time 13.48 ± 2.39 ms, half width 19.67 ± 3.94 ms, decay time 23.70 ± 12.46 ms, n = 48). The OP amplitude evoked during V_{hyp} by apical or basal dendritic stimulation did not change with distance from the soma (Figures S2A and S2B); however, more distally evoked OPs showed longer latencies and slower kinetics (Figures S2E–S2N).

Depolarized Network Activity Reduces the Amplitude of Somatic Inputs in Anesthetized and Awake Mice

ChR2 is a non-specific cation channel that, similar to the glutamate ligand-gated channels, has a reversal potential around 0 mV (Berndt et al., 2011). We therefore expected the amplitude of OPs to be reduced as neurons spontaneously went from V_{hyp} to V_{dep}, based on an expected amplitude reduction in V_{dep} compared to V_{hyp} proportional to $(V_{hyp} - V_{dep})/V_{hyp}$. Indeed, somatically evoked OPs (OP_{som}) of all amplitudes were reduced during V_{dep} (V_{hyp} 1.74 ± 1.21 mV versus V_{dep} 1.4 ± 0.98 mV; n = 27; $p < 0.0001$; Figures 1G and 1I), likely due to the decreased driving force (see STAR Methods; V_{dep} OP amplitude; measured 1.4 ± 0.98 mV versus expected 1.38 ± 0.95 mV; n = 27; p = 0.1482). However, OP_{som} showed a significant increase in the half width (Figure 1H), which may be the result of the increase in input resistance and membrane time constant during V_{dep} (Figures S3A–S3D; Mateo et al., 2011; Waters and Helmchen, 2006). Whereas distinct periods of V_{hyp} and V_{dep} are hallmarks of anesthesia and slow wave sleep (Metherate and Ashe, 1993; Steriade et al., 1993), the V_m of cortical neurons in awake, resting mice also fluctuates between brief, hyperpolarized periods and a depolarized V_m (Poulet and Petersen, 2008). We also observed a reduction in OP_{som} amplitude as neurons went from hyperpolarized to depolarized phases of slow network activity in awake resting mice (Figure 1I).

Weak Basal Dendritic Inputs Are Amplified during Depolarized Network Activity

Excitatory synaptic inputs to pyramidal neurons are targeted to dendrites. We therefore next stimulated basal dendrites and measured responses at the soma (OP_{bas}; Figure 2). Unexpectedly, across all recordings, OP_{bas} amplitude was not significantly different between V_{hyp} to V_{dep} (V_{hyp} 0.39 ± 0.24 mV versus V_{dep} 0.39 ± 0.19 mV; n = 48; p = 0.9150; Figures 2C and 2D), despite the increase in V_m and the expected reduction in amplitude from the reduction in driving force during V_{dep} (V_{dep} amplitude, measured 0.39 ± 0.19 mV versus expected V_{dep} 0.31 ± 0.18 mV; n = 48; p = 0.0001). Like OP_{som}, OP_{bas}

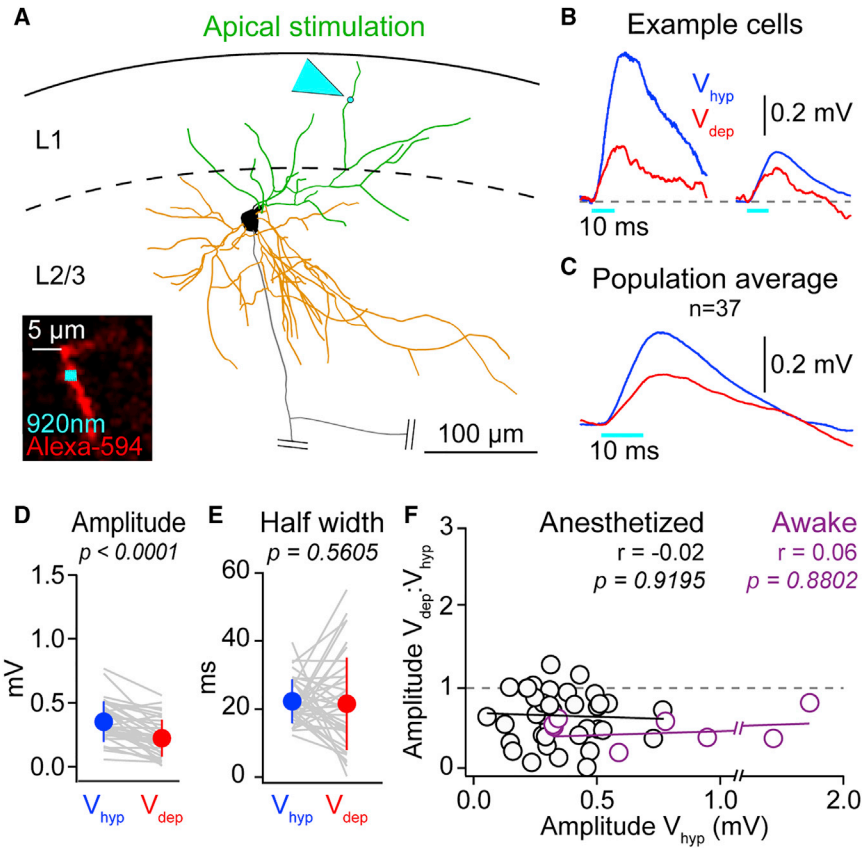

Figure 3. Optogenetic Potentials Evoked by Apical Dendrite Stimulation of Layer 2/3 Pyramidal Neurons Are Reduced in Amplitude during Depolarized Phases of Slow Network Activity

(A) Reconstruction of example layer 2/3 pyramidal neuron showing the soma (black), apical dendrites (green), and basal dendrites (orange), with the apical dendrite two-photon stimulation spot highlighted by cyan arrowhead. Inset shows *in vivo* image of Alexa-Fluor-594-filled dendrite in red and optogenetic stimulation site in cyan.

(B) Overlaid mean OP_{ap} from two example cells shows a reduction in amplitude as neurons go from V_{hyp} (blue) to V_{dep} (red).

(C) Population average OP_{ap} shows reduction in amplitude during V_{dep}.

(D) Amplitude of OP_{ap} is significantly lower in V_{dep} compared to V_{hyp}; gray lines show data from individual cells, filled circles with error bars the mean ± SD.

(E) OP_{ap} half width is not significantly different between V_{hyp} and V_{dep}.

(F) No significant correlation between the ratio of the OP_{ap} amplitude in V_{dep}:V_{hyp} and the OP_{ap} V_{hyp} amplitude in awake (purple) and anesthetized (black). Black and purple lines are linear fits.

showed a significant increase in half width during V_{dep} (half-width, V_{hyp} 19.67 ± 3.94 ms versus V_{dep} 26.19 ± 11.08 ms; n = 48; p = 0.0004; Figure 2E).

To examine this further, we plotted the ratio of the amplitude in V_{dep} to V_{hyp} as a function of the V_{hyp} amplitude (Figure 2F). This revealed that smaller amplitude basal inputs, <0.4 mV, exhibited a significant increase in amplitude in V_{dep} (OP_{bas} < 0.4 mV in V_{hyp}; V_{hyp} 0.24 ± 0.10 mV versus V_{dep} 0.32 ± 0.14 mV; n = 30; p = 0.0002), and larger amplitude responses decreased (OP_{bas} > 0.4 mV; V_{hyp} 0.64 ± 0.19 mV versus V_{dep} 0.50 ± 0.22 mV; n = 18; p = 0.0003; Figures 2B and 2F), resulting in a significant negative correlation. An amplitude-dependent modulation was also observed on the same basal stimulation site with different amplitude stimuli (Figure S4). To confirm that basal input amplification was present in non-anesthetized animals, we repeated stimulation in awake, resting mice (Figure S5). Analysis of OP_{bas} amplitude during the depolarized phase of slow activity revealed a similar correlation as the anesthetized data (Figure 2F): larger amplitude basal inputs decreased, but smaller amplitude inputs increased in amplitude during V_{dep}.

Apical Dendritic Inputs Are Reduced during Depolarized Network Activity

Is the amplification of weak inputs a general feature of synaptic integration in all dendritic compartments of a pyramidal neuron or specific to basal dendrites? We next stimulated apical dendrites (Figure 3) to generate OP_{ap} within the same amplitude range of OP_{bas}. In contrast to OP_{bas}, across the population, OP_{ap} were reduced in amplitude during V_{dep} (V_{hyp} 0.35 ± 0.16 mV versus V_{dep} 0.22 ± 0.14 mV; n = 37; p < 0.0001) and were significantly smaller than expected from the reduction in driving force (V_{dep} OP amplitude, measured 0.22 ± 0.14 mV versus expected 0.28 ± 0.13 mV; n = 37; p = 0.0224). Moreover, the OP_{ap} amplitude ratio between V_{hyp}:V_{dep} was not significantly correlated to the corresponding amplitude during V_{hyp} both in anesthetized and in awake animals (Figure 3F). Therefore, weak apical inputs are not amplified during depolarized network activity. Thus, the modulation of OPs by depolarized network activity is determined by the dendritic input site.

Amplification of Weak Basal Dendrite Targeted Thalamic Input

The increase in weak OP_{bas} amplitude unexpectedly counteracted the reduction in driving force associated with V_{dep}. To confirm whether the amplification of small-amplitude basal inputs is observed during glutamatergic synaptic transmission, we took advantage of the distinct axonal projection patterns of two thalamic nuclei that project to S1, VPM, and POm. VPM axons mostly target layer 4 neurons that subsequently project to the basal dendrites of layer 2/3 neurons (Feldmeyer et al., 2002) but also have axonal collaterals near the border of layer 4 and 2/3 that may directly contact basal dendrites of layer 2/3 neurons (Meyer et al., 2010; Petreanu et al., 2009; Viaene et al., 2011; Wimmer et al., 2010). In contrast, POm neurons project to layer 1 (Meyer et al., 2010; Wimmer et al., 2010), and mapping studies have shown that they provide short latency input to

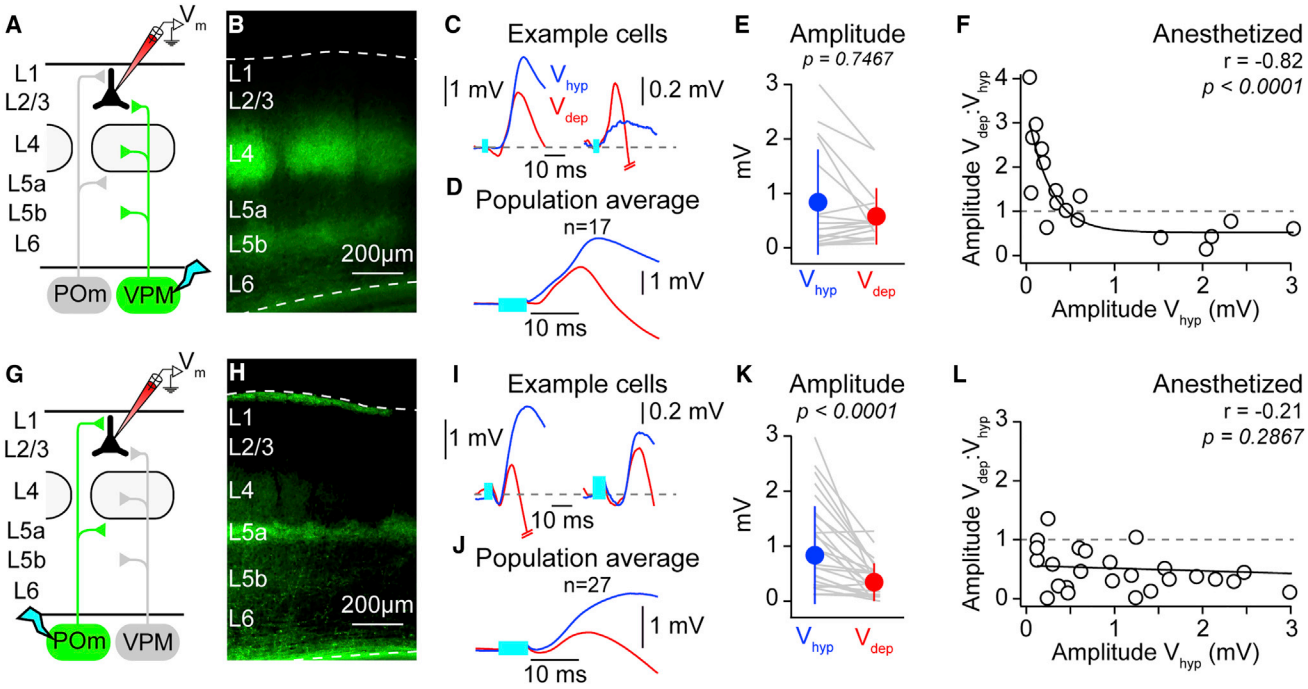

Figure 4. Weak Glutamatergic Thalamic Inputs to Layer 2/3 Pyramidal Neurons from the Ventral Posteromedial Nucleus, but Not the Posteromedial Nucleus, Are Amplified during Depolarized Phases of Slow Network Activity

(A) Cartoon schematic showing ventral posteromedial nucleus (VPM) (green) axonal projections, a light stimulus in the thalamus (cyan), and the recording site.

(B) Example coronal slice of primary somatosensory cortex showing innervation pattern of ChR2-EYFP-expressing VPM thalamic axons; dashed white lines show pial surface and white matter.

(C) Two averaged, overlaid subthreshold responses from a cortical layer 2/3 pyramidal neuron to VPM optogenetic stimulation (cyan bar) during V_{hyp} (blue) and V_{dep} (red) states show (left) a larger amplitude example that decreases during V_{dep} and (right) a smaller amplitude example that increases during V_{dep}.

(D) As in (B) but the population average response.

(E) Across the population, there was no significant difference in the amplitude of responses to VPM stimulation in V_{dep} compared to V_{hyp}. Gray lines show data from individual cells, filled circles with error bars the mean ± SD.

(F) A significant negative correlation between $\log_{10}$ of the VPM-evoked responses during V_{hyp} and the ratio of the V_{dep}:V_{hyp} amplitude, showing the amplification of small-amplitude VPM responses during V_{dep}. Open circles represent mean response from a single cell; black line is a single exponential fit.

(G–L) As for (A)–(F) but for posteromedial nucleus (POm) optogenetic stimulation. Black line in (L) is a linear fit.

layer 2/3 neurons that are thought to be targeted to apical dendritic regions (Audette et al., 2018; Petreanu et al., 2009; Viaene et al., 2011). To activate VPM or POm neurons selectively, we infected VPM or POm with ChR2 and optically stimulated their cell bodies or cortical axons during visually targeted whole-cell recordings from layer 2/3 pyramidal neurons *in vivo* under anesthesia (Figure 4; Jouhanneau et al., 2014).

During V_{dep}, VPM and POm stimulation evoked a short latency depolarizing input and a subsequent hyperpolarization likely due to inhibition from local cortical GABA-ergic neurons. Measurement of the early VPM depolarizing response did not show an overall change in amplitude comparing V_{hyp} to V_{dep} (V_{hyp} 0.84 ± 0.96 mV versus V_{dep} 0.58 ± 0.52 mV; n = 17; p = 0.7467), whereas the early POm response was strongly reduced (V_{hyp} 1.48 ± 1.84 mV versus V_{dep} 0.57 ± 0.73 mV; n = 27; p < 0.0001). Plotting the ratio of the amplitude of the depolarizing response to VPM stimulation in V_{dep}:V_{hyp} against the V_{hyp} amplitude revealed a significant negative correlation (Figure 4F) similar to that observed to direct basal dendrite stimulation (Figure 2F), whereas, like direct apical stimulation (Figure 3F), POm responses showed no correlation (Figure 4L). Thus, these data show that the amplification of weak inputs is a relevant phenomenon for glutamatergic inputs and suggests that weak sensory-evoked glutamatergic input may also be amplified during depolarized network activity (Reig et al., 2015).

Amplification of Small-Amplitude Unitary Monosynaptic EPSPs *In Vivo*

Optogenetic thalamic stimulation activates a large population of presynaptic neurons that evokes network level effects. To measure whether unitary glutamatergic $_u$EPSP also undergo weak input amplification, we performed multiple (2–4) targeted whole-cell recordings from monosynaptically connected layer 2/3 pyramidal neurons *in vivo* (Jouhanneau et al., 2015, 2018), which form the majority of their synaptic contacts on basal dendrites of neighboring excitatory neurons (Feldmeyer et al., 2006; Petreanu et al., 2009). To identify a connection and compare $_u$EPSP amplitude between V_{hyp} and V_{dep}, we evoked single action potentials and measured the postsynaptic response (Figures 5A and 5B). Across 31 connections with a depolarizing

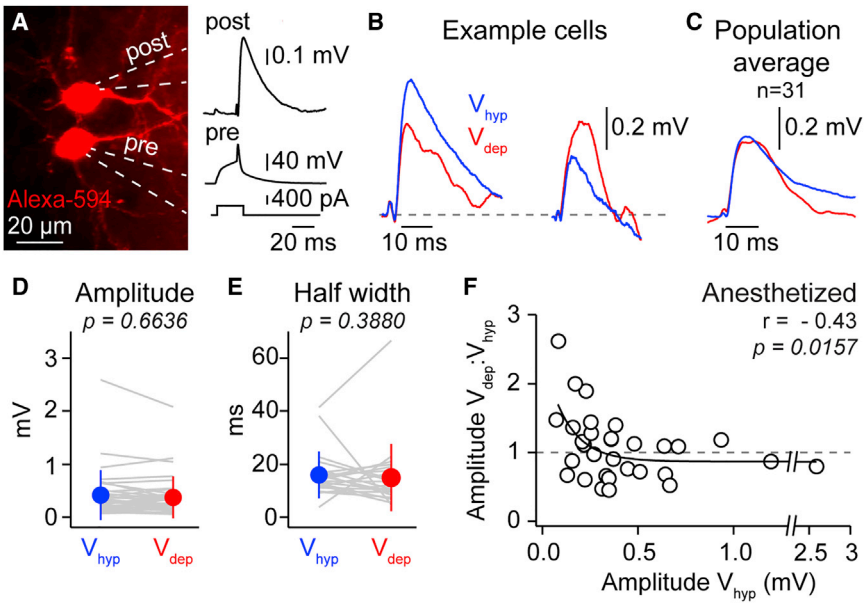

Figure 5. Monosynaptic Glutamatergic Input Modulation by Slow Network Activity

(A) Example *in vivo* two-photon image of two pyramidal neurons stained with Alexa Fluor 594; recording pipettes outlined with white dashed lines; right shows test for monosynaptic connectivity from the same example pair.

(B) Two example, averaged $_u$EPSPs with different V_{hyp} (blue) amplitudes; the larger $_u$EPSP (left) is decreased in V_{dep} (red) whereas the smaller $_u$EPSP is increased (right).

(C) Population-averaged, overlaid $_u$EPSPs during V_{hyp} and V_{dep}.

(D) No change in amplitude of $_u$EPSPs in V_{dep} as compared to V_{hyp} across the population. Gray lines show data from individual cells, filled circles with error bars the mean ± SD.

(E) No change in half width of $_u$EPSPs during V_{dep} and V_{hyp} across the entire population.

(F) Significant correlation between $\log_{10}$ of the V_{hyp} amplitude of $_u$EPSPs and the ratio of amplitude V_{dep}:V_{hyp}, highlighting the amplification of small-amplitude $_u$EPSPs during V_{dep}. Correlations performed on the amplitude ratio V_{dep}:V_{hyp} and $\log_{10}$ of the V_{hyp} $_u$EPSP amplitude are shown. Open circles represent mean response from a single cell; black line is a single exponential fit.

$_u$EPSP in V_{dep} (see STAR Methods), mean $_u$EPSP amplitude and half width were not significantly different during V_{dep} to V_{hyp} (amplitude: V_{hyp} 0.46 ± 0.47 mV versus V_{dep} 0.43 ± 0.39 mV; n = 31 connections; p = 0.6636; Figure 5). Notably, however, smaller amplitude $_u$EPSPs increased in amplitude in V_{dep} and larger amplitude $_u$EPSPs decreased, resulting in a significant negative correlation between the ratio of the $_u$EPSP amplitude in V_{dep}:V_{hyp} and the V_{hyp} amplitude (Figure 5F), similar to the direct basal stimulation and VPM response graphs (Figures 2F and 4F). Thus, amplification of weak inputs is a fundamental feature of the integration of monosynaptic glutamatergic inputs from neighboring layer 2/3 pyramidal neurons *in vivo*.

Basal Input Amplification Is Mediated by Postsynaptic Voltage-Gated Channels

We next returned to basal dendrite optogenetic stimulation to address possible cell-intrinsic, postsynaptic mechanisms underlying the amplification of weak basal inputs (Figure 6A). Cortical slice experiments have shown that $_u$EPSP amplitudes can be modulated by varying the postsynaptic V_m (Deisz et al., 1991; González-Burgos and Barrionuevo, 2001; Markram et al., 1997; Stuart and Sakmann, 1995), suggesting that voltage-gated channels might be important in weak input amplification. We used intracellular antagonists to block different types of voltage-gated channels without affecting local network activity (1 mM MK-801 to block NMDA, 200 µM D-890 to block voltage-dependent Ca^{2+} channels, and 1 mM QX-314 to block voltage-dependent Na^+ channels and, to a minor extent, K^+ channels). Before stimulation, we waited 10 min for the dendrite to be visible and for the drugs to perfuse. During intracellular application of MK-801, D-890, and QX-314, neurons maintained a normal resting V_m and spontaneous subthreshold network activity. Action potential firing, however, was completely absent in QX-314 recordings, due to the block of Na^+ channels.

One possible mechanism underlying the amplification could be that NMDA channels, primed by glutamate release during V_{dep}, are activated by the depolarization of the OP. However, the amplification of weak OP_{bas} was unaffected by the blocking of NMDA channels with MK-801 (Figure 6G). Likewise, blocking of voltage-gated Ca^{2+} channels by D-890 also did not alter basal input amplification (Figure 6G). Inclusion of QX-314 into the intracellular solution, however, had a strong and robust effect. In contrast to control data and recordings with MK-801 or D-890 in the pipette, small-amplitude OP_{bas} were reduced in amplitude during V_{dep} with QX-314 in the pipette (OP_{bas} < 0.4 mV QX-314 V_{hyp} 0.25 ± 0.08 mV versus OP_{bas} < 0.4 mV QX-314 V_{dep} 0.19 ± 0.09 mV; n = 13; p = 0.0171; Figures 6A–6E). Moreover, in contrast to the increase in half width observed in wild-type OP_{bas} (Figure 1H), QX-314 reduced OP_{bas} half width during V_{dep} (Figure 6F). This could be linked to decreased input resistance as neurons transition from V_{hyp} to V_{dep} in QX-314-treated neurons (Figures S3E–S3G; Remme and Rinzel, 2011; Waters and Helmchen, 2006). Plotting the ratio of the amplitude of the OP_{bas} response in V_{dep}:V_{hyp} against the OP_{bas} V_{hyp} amplitude during QX-314 application showed no significant correlation (Figure 6G). Thus, only QX-314 blocked the boosting of small OP_{bas} during network activity (Figure 6H). Together, our data suggest that postsynaptic voltage-gated channels are required for the amplification of small-amplitude basal inputs during depolarized network activity *in vivo*.

Modeling a Postsynaptic Voltage-Gated Channel-Dependent Mechanism

If basal input amplification is achieved via a postsynaptic voltage-gated ion channel (VGC), what are the activation, kinetics, and

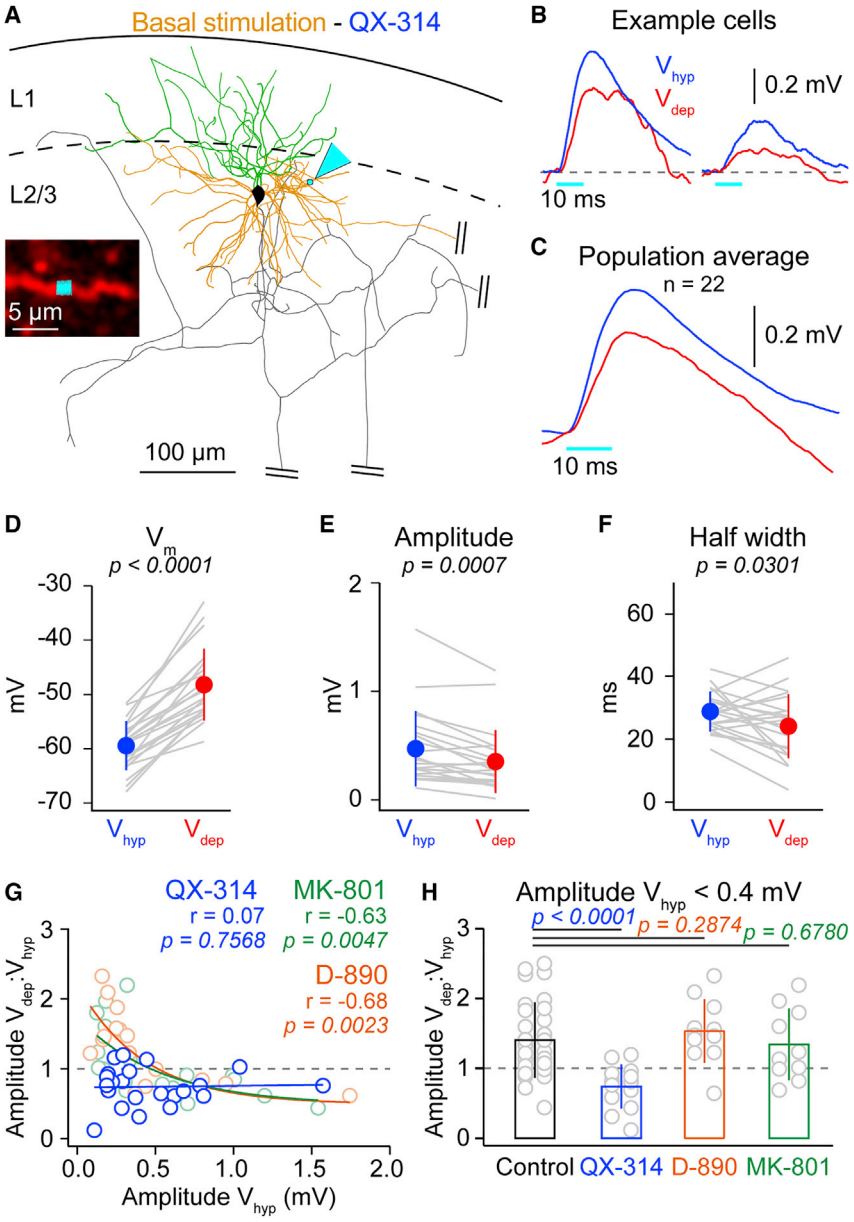

Figure 6. Amplification of Weak Basal Inputs Is Blocked by Intracellular Application of QX-314

(A) Biocytin reconstruction of example cell from basal dendrite optogenetic stimulation experiment, showing the apical (green) and basal (orange) dendrite, the axon (gray, truncated), and the optogenetic stimulation spot (cyan arrow). Inset shows *in vivo* image of Alexa-Fluor-594-filled dendrite in red and optogenetic stimulation site in cyan.

(B) Both large- and small-amplitude mean example OP_{bas} show a reduction in amplitude from V_{hyp} (blue) to V_{dep} (red) during whole-cell recordings with 1 mM QX-314 in intracellular solution.

(C) Population mean OP_{bas} during intracellular QX-314 application is reduced in V_{dep}.

(D) V_m increase as neurons transition from V_{hyp} to V_{dep} during experiments using intracellular QX-314. Gray lines show data from individual cells, filled circles with error bars the mean ± SD.

(E) A significant reduction of OP_{bas} amplitude in V_{dep} compared to V_{hyp}.

(F) OP_{bas} half width is significantly smaller in V_{dep} in comparison with V_{hyp}.

(G) No correlation between state modulation of OP_{bas} amplitude and the $\log_{10}$ of V_{hyp} OP amplitude during QX-314 application (blue); significant correlation during MK-801 (light green) and D-890 (light orange) application. Open circles represent mean response from a single cell, blue line shows linear fit, and green and orange lines single exponential fit.

(H) The ratios of the V_{dep}:V_{hyp} amplitude for small-amplitude OP_{bas} (<0.4 mV) are significantly different during intracellular QX-314 application, but not during MK-801 or D-890. Gray open circles show data from single cells; bars show mean ± SD.

anatomical distribution requirements of channels that could underlie this effect? We developed a compartmental model of a reconstructed layer 2/3 pyramidal neuron (Figure 7A; see STAR Methods) to address these questions. Based on the results of pharmacological blocking, we hypothesized the involvement of an amplifying current, i.e., a voltage-gated current that amplifies voltage changes in a certain subthreshold voltage regime (see Remme and Rinzel, 2011). Typical examples of such currents are the persistent Na^+ current, a low-threshold activated Ca^{2+} current, or NMDA receptor currents. Assuming that the putative VGC activates in a voltage range between V_{hyp} and V_{dep} (−60 to −50 mV), but not far below, the current can account for the amplification of weak basal inputs in the following way (Figure 7B): at V_{hyp}, weak input to a basal dendrite (blue traces, left column) is not able to significantly activate the channel and leads to a small response at the soma (bottom panel). Strong input (blue traces, right column), on the other hand, activates the current during V_{hyp}, leading to much larger responses at the soma. At V_{dep} (red traces), both weak and strong inputs activate the voltage-gated current in the basal dendrites, leading to a proportionally larger response to weak inputs.

We quantitatively modeled current properties that might be necessary to account for our results (Figure 7C) by varying the voltage dependence and kinetics of the hypothetical current, as well as its density and distribution across the cell over physiologically plausible ranges (see STAR Methods). For each parameter combination, we simulated basal input during V_{hyp} and V_{dep}, recorded the somatic voltage response, and compared the response amplitude to the experimental observations (Figure 7C). The data were well fit by a group of parameter settings (Figures 7 and S6) that all shared the following features: the current was activated in a voltage range above V_{hyp} (>−60 mV), it activated faster than the membrane time constant, and the channels were distributed across the distal basal dendrites (>70 µm from the soma; see blue dendritic branches in

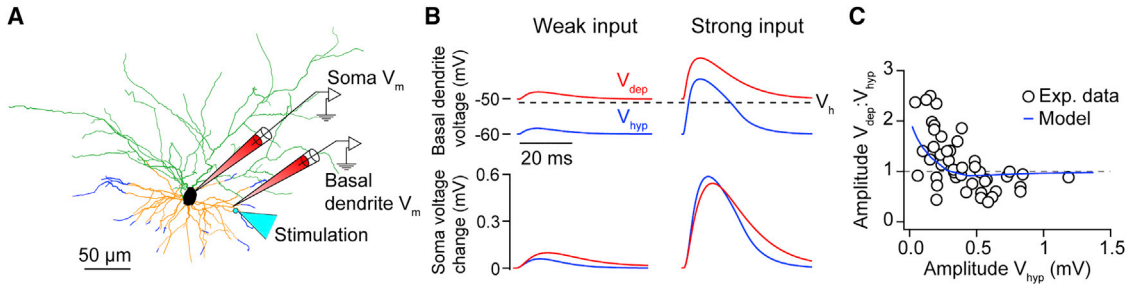

Figure 7. Model Analysis Identifies a Potential Mechanism Underlying the Amplification of Weak Basal Inputs based on Voltage-Dependent Currents

(A) Layer 2/3 pyramidal cell model; location of the simulated input is indicated by a cyan circle and arrow in the basal dendrites (orange); location of the simulated V_m recordings is indicated by two electrodes on the soma and on a basal dendrite close to the input stimulation; distal segments of the basal dendrites express a VGC (dark blue).

(B) Voltage response to input in basal dendrites (basal dendrite electrode in A) recorded at the location of the stimulus (top) and at the soma (bottom; see soma electrode in A). Responses are shown to weak (left) and strong (right) input in both V_{dep} (red curves) and V_{hyp} (blue traces). Black dotted line in top panels marks the half-activation voltage, V_h, of the current (see STAR Methods and Figure S6B). Dotted line in top panels marks the half-activation voltage of the current (see Figure S6B). Soma voltage change with respect to holding voltage (−60 mV for V_{hyp} or −50 mV for V_{dep}) is shown.

(C) Ratio of somatic amplitudes in V_{dep} versus V_{hyp} shown as a function of the V_{dep} amplitudes for basal input. Both model results (blue curve) and experimental data (open circles) are shown.

Figure 7A), ensuring that the active current only affects basal inputs and not the somatic inputs (Zhuchkova et al., 2013). Together with the pharmacology, this model provides support for a postsynaptic VGC mechanism to underlie the amplification of basal input and suggests suitable kinetics and subcellular distributions.

DISCUSSION

Here, we compared the integration of excitatory synaptic inputs in apical versus basal dendrites of layer 2/3 primary somatosensory cortex pyramidal neurons *in vivo*. Because layer 2/3 pyramidal neurons fire sparsely, often with single action potentials (Barth and Poulet, 2012), we examined the postsynaptic responses to single inputs. We show that weak inputs from basal dendrites are amplified whereas inputs of all amplitudes from apical dendrites are attenuated during slow depolarized network activity. This was true not only of direct optogenetically evoked responses but also of thalamic and monosynaptic cortical glutamatergic inputs. Amplification of weak basal inputs could be blocked with an intracellular voltage-dependent ion channel antagonist, and compartmental modeling identified a plausible voltage-dependent channel mechanism. Together, our findings highlight an unexpected dendritic region specificity in the impact of depolarized network activity on synaptic integration *in vivo*.

Two-Photon Subcellular Optogenetic Stimulation as a Tool for Studying Synaptic Integration *In Vivo*

Synaptic integration *in vivo* involves the processing of spatially separated dendritic inputs during depolarized network activity. Whereas the location of active dendritic inputs can be now identified with functional imaging (Chen et al., 2013; Jia et al., 2010), the integration of subthreshold inputs with network activity *in vivo* has typically been studied without identification of the input site using sensory (Chadderton et al., 2014; Crochet et al., 2011; Longordo et al., 2013; Reig et al., 2015; Sachdev et al., 2004), electrical (Reig et al., 2015; Sachdev et al., 2004), or optogenetic stimulation (Mateo et al., 2011; Pala and Petersen, 2015, 2018) or simultaneous recordings (Bruno and Sakmann, 2006; Crochet et al., 2005; Jouhanneau et al., 2018). Two-photon glutamate uncaging allows location-specific control of synaptic inputs and has been used in silenced networks *in vivo* (Noguchi et al., 2011), but its use in active networks is limited because the caged compound can act as an antagonist of GABA transmission (Maier et al., 2005). Channelrhodopsin2 can be expressed in genetically defined cell types, thus avoiding non-specific activation of inhibitory inputs, and can be rapidly activated by two-photon light stimulation (Packer et al., 2012; Prakash et al., 2012). Similar to measurements of simulated dendritic input in cortical slice experiments, the latency and time course of evoked OPs are correlated with the distance of the input site from the soma. Within 135 µm from the soma, we did not observe a correlation of OP amplitude with distance resembling prior cortical slice experiments using simultaneous somatic and basal dendritic recordings (Nevian et al., 2007). Although the rise time of an OP is slightly slower than a glutamatergic $_u$EPSP, future experiments could use ChR2 variants with faster kinetics. These data, alongside the similarities between the modulation of OPs and monosynaptic glutamatergic inputs (Figure 5) by network activity, support the use of this method to further investigate synaptic integration *in vivo* under different behavioral and cortical states.

Cortical Depolarized Network Activity Amplifies Weak Inputs to Basal Dendrites

Spontaneous network activity dominates the membrane potential of cortical neurons and has been observed in direct dendritic recordings *in vivo* (Waters and Helmchen, 2004), but its impact on synaptic integration is still debated. A central result of our study is that network activity reweights apical and basal inputs separately, suppressing apical but enhancing weak basal inputs (Figures 2 and 3). Such an amplification is also present for glutamatergic inputs from VPM and neighboring pyramidal neurons

(Figures 4 and 5), two sources of synaptic inputs thought to target basal dendrites of layer 2/3 pyramidal neurons (Feldmeyer et al., 2006; Meyer et al., 2010; Petreanu et al., 2009). At first glance, this result appears counterintuitive. The increase in EPSP amplitude goes against the reduction in driving force during V_{dep} and the increased membrane conductance. However, an increase of OP_{bas} amplitude at more depolarized potentials resembles the voltage dependency of evoked and dendritically simulated EPSPs in cortical slice experiments (Andreasen and Lambert, 1999; Deisz et al., 1991; González-Burgos and Barrionuevo, 2001; Markram et al., 1997; Stuart and Sakmann, 1995). Moreover, the broadening of OP_{bas} half width during V_{dep} goes together with the increase in input resistance observed in V_{dep} (Figures 2 and S3; Mateo et al., 2011; Waters and Helmchen, 2006).

To examine whether postsynaptic voltage-dependent ion channels were involved in basal input amplification without affecting network activity required intracellular antagonists. Our experiments show that basal input amplification could be blocked by application of the VGC blocker QX-314. A modeling approach suggested that the putative channel should be localized in distal basal dendrites, activate close to V_{dep} (at around −50 mV), and be activated faster than the membrane time constant. The hypothesized activation function of the putative current ensures that, at hyperpolarized potentials, strong basal dendritic inputs are required for channel opening and the resulting amplification, and weak inputs do not suffice. In contrast, at depolarized potentials, both weak and strong basal inputs are amplified by the current. As a consequence, response amplitudes to weak and strong inputs differ strongly in the hyperpolarized state, and the difference is much reduced in the depolarized state.

Reduction in Apical and Somatic Responses during Depolarized Network Activity

As predicted in models and observed in cortical slices during conductance injection (Bernander et al., 1991; Destexhe and Paré, 1999; Destexhe et al., 2003; Williams, 2004), the somatic impact of somatic and apical dendritic inputs is reduced during network activity with the apical responses reduced more than expected based on the change in driving force. So, alongside the increase in conductance, what mechanisms could reduce apical inputs during depolarized activity? Somatostatin-expressing GABA-ergic inhibitory interneurons are thought to contact apical dendritic regions of pyramidal neurons (Jiang et al., 2013); hence, one hypothesis could be that apical dendrite targeting inhibitory interneurons shunt apically evoked $_{u}$EPSPs as they propagate to the soma. If this were the case, significant differences in the impact of apical inputs on the somatic voltage during periods of movement should occur, as somatostatin-expressing neurons are known to be strongly modulated by behavioral state (Gentet et al., 2012; Muñoz et al., 2017). Testing this prediction will require rapid manipulation of somatostatin-expressing neurons activity during apical dendritic stimulation.

Functional Impact on Sensory Processing and Synaptic Integration

Cortical network activity is known to have a fundamental impact on cortical sensory processing (Chance et al., 2002; Petersen et al., 2003; Sachdev et al., 2004; Shu et al., 2003). Our thalamic optogenetic stimulation data predict that the cortical synaptic response to weak somatosensory stimuli, going via VPM to the cortex, would be amplified and may help in the perceptual detection of weak tactile inputs. In support of this proposal, a recent study found a comparable amplification of weak subthreshold inputs during low-intensity acoustic stimulation in depolarized states (Reig et al., 2015). Reig et al. (2015) concluded that the effect was likely the result of a combination of an increase in postsynaptic membrane conductance and in the presynaptic recruitment of additional inhibitory inputs during V_{dep}. We suggest that postsynaptic voltage-dependent channels also play a major role in boosting the cortical representation of weak sensory inputs during depolarized network activity.

Conclusions and Future Work

Axo-dendritic synaptic connections from local layer 2/3 cortical excitatory neurons are mostly formed on basal dendrites (Feldmeyer et al., 2006; Petreanu et al., 2009), whereas inputs from distant cortical neurons and higher order thalamic nuclei terminate in cortical layer 1, likely targeting apical dendrites (Meyer et al., 2010; Petreanu et al., 2009; Veinante and Deschênes, 2003; Wimmer et al., 2010). Thus, slow cortical network activity appears to dynamically alter the relative contribution of distinct synaptic information to the soma of pyramidal neurons.

Our findings suggest that, during slow cortical activity in resting animals, bottom-up, sensory, and local input dominates the somatic response. Recent work has observed an increase in EPSP amplitude to cortical GABA-ergic interneurons during movement (Pala and Petersen, 2018), and one possibility is that higher order and top-down apical inputs to pyramidal neurons may play a more dominant role in somatic integration and spike generation during desynchronized cortical activity. Future work must therefore now assess the relative impact of apical and basal inputs in attentive and behaving mice.

STAR★METHODS

Detailed methods are provided in the online version of this paper and include the following:

- KEY RESOURCES TABLE
- CONTACT FOR REAGENT AND RESOURCE SHARING
- EXPERIMENTAL MODEL AND SUBJECT DETAILS
- METHOD DETAILS
  - Surgery and intrinsic optical imaging
  - Virus injections
  - Two-photon targeted whole-cell patch clamp recordings
  - Subcellular two-photon optogenetic stimulation
  - Histology
  - Electrophysiological inclusion parameters
  - Compartmental model
- QUANTIFICATION AND STATISTICAL ANALYSIS
  - Datasets
  - Selection of V_{hyp}/V_{dep}
  - Amplitude measurement of subthreshold responses
  - Input resistance
  - *In vivo* data statistics

SUPPLEMENTAL INFORMATION

Supplemental Information includes six figures and can be found with this article online at https://doi.org/10.1016/j.celrep.2018.08.088.

ACKNOWLEDGMENTS

We thank Janett König for technical help and Alison Barth, Evgeny Bobrov, and Philipp Schnepel for comments on an earlier version of the manuscript. This work was funded by the European Research Council (ERC-2010-StG-260590 and ERC-2015-CoG-682422; J.F.A.P.), the Deutsche Forschungsgemeinschaft (DFG) (Exc 257 NeuroCure, DFG-FOR-1341-BaCoFun, and DFG-FOR-2143-Interneuron; J.F.A.P.), the Thyssen Foundation, the European Union's FP7 Programme (3x3Dimaging 323945; J.F.A.P.), the Helmholtz Association (J.F.A.P.), and the Bundesministerium für Bildung und Forschung (01GQ0901 and 01GQ1403; S.S.). B.R. was funded by the European Research Council (ERC 682426), and B.R. and K.G. by the Hungarian National Research, Development and Innovation Office (KFI_16-1-2016-0177, GINOP_2.1.1-15-2016-00979, VKSZ_14-1-2015-0155, and NAP-2.0/VIII/2), and the European Union's Horizon (712821) and FP7 (ICT-2011-C 323945) programs. J.K. was funded by the Humboldt-Universität zu Berlin in the framework of the Excellence Initiative of the BMBF and DFG (Emmy-Noether KR 4062/4–1).

AUTHOR CONTRIBUTIONS

Conceptualization, L.F., J.-S.J., and J.F.A.P.; Methodology, L.F., B.R., G.K., and M.W.H.R.; Investigation, L.F., J.-S.J., and M.W.H.R.; Formal Analysis, L.F., J.-S.J., M.W.H.R., and J.K.; Writing – Original Draft, J.F.A.P.; Writing – Review & Editing, L.F., J.-S.J., M.W.H.R., S.S., and J.F.A.P.; Resources, S.S. and J.F.A.P.; Visualization, L.F., J.-S.J., M.W.H.R., and J.F.A.P.; Supervision, S.S. and J.F.A.P.; Funding Acquisition, B.R., G.K., J.K., S.S., and J.F.A.P.

DECLARATION OF INTERESTS

G.K. and B.R. are founders of Femtonics Kft. B.R. is a member of its scientific advisory board.

Received: July 6, 2017
Revised: April 24, 2018
Accepted: August 29, 2018
Published: September 25, 2018

REFERENCES

Andreasen, M., and Lambert, J.D. (1999). Somatic amplification of distally generated subthreshold EPSPs in rat hippocampal pyramidal neurones. J. Physiol. *519*, 85–100.

Audette, N.J., Urban-Ciecko, J., Matsushita, M., and Barth, A.L. (2018). POm thalamocortical input drives layer-specific microcircuits in somatosensory cortex. Cereb. Cortex *28*, 1312–1328.

Barth, A.L., and Poulet, J.F.A. (2012). Experimental evidence for sparse firing in the neocortex. Trends Neurosci. *35*, 345–355.

Bernander, O., Douglas, R.J., Martin, K.A., and Koch, C. (1991). Synaptic background activity influences spatiotemporal integration in single pyramidal cells. Proc. Natl. Acad. Sci. USA *88*, 11569–11573.

Berndt, A., Schoenenberger, P., Mattis, J., Tye, K.M., Deisseroth, K., Hegemann, P., and Oertner, T.G. (2011). High-efficiency channelrhodopsins for fast neuronal stimulation at low light levels. Proc. Natl. Acad. Sci. USA *108*, 7595–7600.

Bruno, R.M., and Sakmann, B. (2006). Cortex is driven by weak but synchronously active thalamocortical synapses. Science *312*, 1622–1627.

Chadderton, P., Schaefer, A.T., Williams, S.R., and Margrie, T.W. (2014). Sensory-evoked synaptic integration in cerebellar and cerebral cortical neurons. Nat. Rev. Neurosci. *15*, 71–83.

Chance, F.S., Abbott, L.F., and Reyes, A.D. (2002). Gain modulation from background synaptic input. Neuron *35*, 773–782.

Chen, X., Rochefort, N.L., Sakmann, B., and Konnerth, A. (2013). Reactivation of the same synapses during spontaneous up states and sensory stimuli. Cell Rep. *4*, 31–39.

Cowan, R.L., and Wilson, C.J. (1994). Spontaneous firing patterns and axonal projections of single corticostriatal neurons in the rat medial agranular cortex. J. Neurophysiol. *71*, 17–32.

Crochet, S., Chauvette, S., Boucetta, S., and Timofeev, I. (2005). Modulation of synaptic transmission in neocortex by network activities. Eur. J. Neurosci. *21*, 1030–1044.

Crochet, S., Poulet, J.F.A., Kremer, Y., and Petersen, C.C.H. (2011). Synaptic mechanisms underlying sparse coding of active touch. Neuron *69*, 1160–1175.

Deisz, R.A., Fortin, G., and Zieglgänsberger, W. (1991). Voltage dependence of excitatory postsynaptic potentials of rat neocortical neurons. J. Neurophysiol. *65*, 371–382.

Destexhe, A., and Paré, D. (1999). Impact of network activity on the integrative properties of neocortical pyramidal neurons in vivo. J. Neurophysiol. *81*, 1531–1547.

Destexhe, A., Rudolph, M., and Paré, D. (2003). The high-conductance state of neocortical neurons in vivo. Nat. Rev. Neurosci. *4*, 739–751.

Feldmeyer, D., Lübke, J., Silver, R.A., and Sakmann, B. (2002). Synaptic connections between layer 4 spiny neurone-layer 2/3 pyramidal cell pairs in juvenile rat barrel cortex: physiology and anatomy of interlaminar signalling within a cortical column. J. Physiol. *538*, 803–822.

Feldmeyer, D., Lübke, J., and Sakmann, B. (2006). Efficacy and connectivity of intracolumnar pairs of layer 2/3 pyramidal cells in the barrel cortex of juvenile rats. J. Physiol. *575*, 583–602.

Gentet, L.J., Kremer, Y., Taniguchi, H., Huang, Z.J., Staiger, J.F., and Petersen, C.C.H. (2012). Unique functional properties of somatostatin-expressing GABAergic neurons in mouse barrel cortex. Nat. Neurosci. *15*, 607–612.

Goebbels, S., Bormuth, I., Bode, U., Hermanson, O., Schwab, M.H., and Nave, K.-A. (2006). Genetic targeting of principal neurons in neocortex and hippocampus of NEX-Cre mice. Genesis *44*, 611–621.

González-Burgos, G., and Barrionuevo, G. (2001). Voltage-gated sodium channels shape subthreshold EPSPs in layer 5 pyramidal neurons from rat prefrontal cortex. J. Neurophysiol. *86*, 1671–1684.

Hines, M.L., and Carnevale, N.T. (1997). The NEURON simulation environment. Neural Comput. *9*, 1179–1209.

Jia, H., Rochefort, N.L., Chen, X., and Konnerth, A. (2010). Dendritic organization of sensory input to cortical neurons in vivo. Nature *464*, 1307–1312.

Jiang, X., Wang, G., Lee, A.J., Stornetta, R.L., and Zhu, J.J. (2013). The organization of two new cortical interneuronal circuits. Nat. Neurosci. *16*, 210–218.

Jouhanneau, J.-S., Ferrarese, L., Estebanez, L., Audette, N.J., Brecht, M., Barth, A.L., and Poulet, J.F.A. (2014). Cortical fosGFP expression reveals broad receptive field excitatory neurons targeted by POm. Neuron *84*, 1065–1078.

Jouhanneau, J.-S., Kremkow, J., Dorrn, A.L., and Poulet, J.F.A. (2015). In vivo monosynaptic excitatory transmission between layer 2 cortical pyramidal neurons. Cell Rep. *13*, 2098–2106.

Jouhanneau, J.-S., Kremkow, J., and Poulet, J.F.A. (2018). Single synaptic inputs drive high-precision action potentials in parvalbumin expressing GABA-ergic cortical neurons in vivo. Nat. Commun. *9*, 1540–1550.

Lefort, S., Tomm, C., Floyd Sarria, J.-C., and Petersen, C.C.H. (2009). The excitatory neuronal network of the C2 barrel column in mouse primary somatosensory cortex. Neuron *61*, 301–316.

Longordo, F., To, M.-S., Ikeda, K., and Stuart, G.J. (2013). Sublinear integration underlies binocular processing in primary visual cortex. Nat. Neurosci. *16*, 714–723.

Magee, J.C. (2000). Dendritic integration of excitatory synaptic input. Nat. Rev. Neurosci. *1*, 181–190.

Maier, W., Corrie, J.E.T., Papageorgiou, G., Laube, B., and Grewer, C. (2005). Comparative analysis of inhibitory effects of caged ligands for the NMDA receptor. J. Neurosci. Methods *142*, 1–9.

Markram, H., Lübke, J., Frotscher, M., Roth, A., and Sakmann, B. (1997). Physiology and anatomy of synaptic connections between thick tufted pyramidal neurones in the developing rat neocortex. J. Physiol. *500*, 409–440.

Markram, H., Toledo-Rodriguez, M., Wang, Y., Gupta, A., Silberberg, G., and Wu, C. (2004). Interneurons of the neocortical inhibitory system. Nat. Rev. Neurosci. *5*, 793–807.

Mateo, C., Avermann, M., Gentet, L.J., Zhang, F., Deisseroth, K., and Petersen, C.C.H. (2011). In vivo optogenetic stimulation of neocortical excitatory neurons drives brain-state-dependent inhibition. Curr. Biol. *21*, 1593–1602.

Metherate, R., and Ashe, J.H. (1993). Ionic flux contributions to neocortical slow waves and nucleus basalis-mediated activation: whole-cell recordings in vivo. J. Neurosci. *13*, 5312–5323.

Meyer, H.S., Wimmer, V.C., Hemberger, M., Bruno, R.M., de Kock, C.P.J., Frick, A., Sakmann, B., and Helmstaedter, M. (2010). Cell type-specific thalamic innervation in a column of rat vibrissal cortex. Cereb. Cortex *20*, 2287–2303.

Milenkovic, N., Zhao, W.-J., Walcher, J., Albert, T., Siemens, J., Lewin, G.R., and Poulet, J.F.A. (2014). A somatosensory circuit for cooling perception in mice. Nat. Neurosci. *17*, 1560–1566.

Muñoz, W., Tremblay, R., Levenstein, D., and Rudy, B. (2017). Layer-specific modulation of neocortical dendritic inhibition during active wakefulness. Science *355*, 954–959.

Nevian, T., Larkum, M.E., Polsky, A., and Schiller, J. (2007). Properties of basal dendrites of layer 5 pyramidal neurons: a direct patch-clamp recording study. Nat. Neurosci. *10*, 206–214.

Noguchi, J., Nagaoka, A., Watanabe, S., Ellis-Davies, G.C.R., Kitamura, K., Kano, M., Matsuzaki, M., and Kasai, H. (2011). In vivo two-photon uncaging of glutamate revealing the structure-function relationships of dendritic spines in the neocortex of adult mice. J. Physiol. *589*, 2447–2457.

Packer, A.M., Peterka, D.S., Hirtz, J.J., Prakash, R., Deisseroth, K., and Yuste, R. (2012). Two-photon optogenetics of dendritic spines and neural circuits. Nat. Methods *9*, 1202–1205.

Pala, A., and Petersen, C.C.H. (2015). In vivo measurement of cell-type-specific synaptic connectivity and synaptic transmission in layer 2/3 mouse barrel cortex. Neuron *85*, 68–75.

Pala, A., and Petersen, C.C. (2018). State-dependent cell-type-specific membrane potential dynamics and unitary synaptic inputs in awake mice. eLife *7*, 350.

Petersen, C.C.H., Hahn, T.T.G., Mehta, M., Grinvald, A., and Sakmann, B. (2003). Interaction of sensory responses with spontaneous depolarization in layer 2/3 barrel cortex. Proc. Natl. Acad. Sci. USA *100*, 13638–13643.

Petreanu, L., Mao, T., Sternson, S.M., and Svoboda, K. (2009). The subcellular organization of neocortical excitatory connections. Nature *457*, 1142–1145.

Poulet, J.F.A., and Petersen, C.C.H. (2008). Internal brain state regulates membrane potential synchrony in barrel cortex of behaving mice. Nature *454*, 881–885.

Prakash, R., Yizhar, O., Grewe, B., Ramakrishnan, C., Wang, N., Goshen, I., Packer, A.M., Peterka, D.S., Yuste, R., Schnitzer, M.J., and Deisseroth, K. (2012). Two-photon optogenetic toolbox for fast inhibition, excitation and bistable modulation. Nat. Methods *9*, 1171–1179.

Reig, R., Zerlaut, Y., Vergara, R., Destexhe, A., and Sanchez-Vives, M.V. (2015). Gain modulation of synaptic inputs by network state in auditory cortex in vivo. J. Neurosci. *35*, 2689–2702.

Remme, M.W.H., and Rinzel, J. (2011). Role of active dendritic conductances in subthreshold input integration. J. Comput. Neurosci. *31*, 13–30.

Sachdev, R.N.S., Ebner, F.F., and Wilson, C.J. (2004). Effect of subthreshold up and down states on the whisker-evoked response in somatosensory cortex. J. Neurophysiol. *92*, 3511–3521.

Shu, Y., Hasenstaub, A., Badoual, M., Bal, T., and McCormick, D.A. (2003). Barrages of synaptic activity control the gain and sensitivity of cortical neurons. J. Neurosci. *23*, 10388–10401.

Song, S., Sjöström, P.J., Reigl, M., Nelson, S., and Chklovskii, D.B. (2005). Highly nonrandom features of synaptic connectivity in local cortical circuits. PLoS Biol. *3*, e68.

Spruston, N. (2008). Pyramidal neurons: dendritic structure and synaptic integration. Nat. Rev. Neurosci. *9*, 206–221.

Steriade, M., Nuñez, A., and Amzica, F. (1993). A novel slow (< 1 Hz) oscillation of neocortical neurons in vivo: depolarizing and hyperpolarizing components. J. Neurosci. *13*, 3252–3265.

Stuart, G., and Sakmann, B. (1995). Amplification of EPSPs by axosomatic sodium channels in neocortical pyramidal neurons. Neuron *15*, 1065–1076.

Tamamaki, N., Yanagawa, Y., Tomioka, R., Miyazaki, J., Obata, K., and Kaneko, T. (2003). Green fluorescent protein expression and colocalization with calretinin, parvalbumin, and somatostatin in the GAD67-GFP knock-in mouse. J. Comp. Neurol. *467*, 60–79.

Veinante, P., and Deschênes, M. (2003). Single-cell study of motor cortex projections to the barrel field in rats. J. Comp. Neurol. *464*, 98–103.

Viaene, A.N., Petrof, I., and Sherman, S.M. (2011). Properties of the thalamic projection from the posterior medial nucleus to primary and secondary somatosensory cortices in the mouse. Proc. Natl. Acad. Sci. USA *108*, 18156–18161.

Waters, J., and Helmchen, F. (2004). Boosting of action potential backpropagation by neocortical network activity in vivo. J. Neurosci. *24*, 11127–11136.

Waters, J., and Helmchen, F. (2006). Background synaptic activity is sparse in neocortex. J. Neurosci. *26*, 8267–8277.

Williams, S.R. (2004). Spatial compartmentalization and functional impact of conductance in pyramidal neurons. Nat. Neurosci. *7*, 961–967.

Williams, S.R., and Stuart, G.J. (2002). Dependence of EPSP efficacy on synapse location in neocortical pyramidal neurons. Science *295*, 1907–1910.

Wimmer, V.C., Bruno, R.M., de Kock, C.P.J., Kuner, T., and Sakmann, B. (2010). Dimensions of a projection column and architecture of VPM and POm axons in rat vibrissal cortex. Cereb. Cortex *20*, 2265–2276.

Zhao, W.-J., Kremkow, J., and Poulet, J.F.A. (2016). Translaminar cortical membrane potential synchrony in behaving mice. Cell Rep. *15*, 2387–2399.

Zhuchkova, E., Remme, M.W.H., and Schreiber, S. (2013). Somatic versus dendritic resonance: differential filtering of inputs through non-uniform distributions of active conductances. PLoS ONE *8*, e78908.

STAR★METHODS

KEY RESOURCES TABLE

REAGENT or RESOURCE	SOURCE	IDENTIFIER
Bacterial and Virus Strains		
AAV2/9 pAAV-αCaMKII-hChR2(T159C)-p2A-EYFP	Charité Vector Core	VCA-43a
AAV2/9 pAAV-αCaMKII-hChR2(E123T/T159C)-p2A-EYFP	Charité Vector Core	BA-150a
pLenti-Synapsin-hChR2(H134R)-EYFP	Charité Vector Core	BLV-679
Chemicals, Peptides, and Recombinant Proteins		
NaCl	Sigma-Aldrich	S7653
KCl	Sigma-Aldrich	P9333
HEPES	Sigma-Aldrich	H3375
MgCl2*6H2O	Sigma-Aldrich	M2670
CaCl2*2H2O	Sigma-Aldrich	C5080
NaOH	Sigma-Aldrich	S8045
Potassium D-gluconate	Sigma-Aldrich	G4500
KCl	Sigma-Aldrich	P9333
Adenosine 5′-triphosphate magnesium salt	Sigma-Aldrich	A9187
Phosphocreatine disodium salt hydrate	Sigma-Aldrich	P7936
Guanosine 5′-triphosphate sodium salt hydrate	Sigma-Aldrich	G8877
HEPES	Sigma-Aldrich	H3375
KOH	Sigma-Aldrich	P5958
Biocytin	Tocris	3349
QX-314 bromide	Tocris	1014
(+)-MK-801 maleate	Tocris	0924
D-890	Abcam	ab120333
Alexa Fluor 594	ThermoFisher	A10438
Urethane	Sigma-Aldrich	U2500
Metamizol	Zentiva	416485
Isoflurane	Cp-pharma	1214
Ketamine 10%	WDT	9089.01.00
Rompun 2% Xylazin	Bayer	KP0CTJS
Vectastain Elite ABC-Peroxidase kit	Biozol	VEC-PK-6100
Denture acrylic	Heraeus	64707963
Agarose, Type III-A	Sigma-Aldrich	A9793
Mowiol	Sigma-Aldrich	81381
Roti-Histofix 4% (PFA)	Roth	P087.4
Sodium phosphate monobasic dihydrate	Sigma-Aldrich	71505
Sodium phosphate monobasic monohydrate	Sigma-Aldrich	S9638
Sodium phosphate dibasic dihydrate	Sigma-Aldrich	71643
Experimental Models: Organisms/Strains		
Mouse-C57BL/6J	FEM Charité	C57BL/6J
Mouse-Nex-cre	Klaus Nave	Nex-cre
Mouse-Ai9	The Jackson Lab	007909
Mouse-GAD67-GFP	Yuchio Yanagawa	GAD67-GFP
Mouse-fosGFP	The Jackson Lab	014135

(*Continued on next page*)

Continued

REAGENT or RESOURCE	SOURCE	IDENTIFIER
Software and Algorithms		
IGORpro 6	Wavemetrics	https://www.wavemetrics.com
MATLAB	MathWorks	https://www.mathworks.com
NEURON	NEURON	https://neuron.yale.edu/neuron
Neurolucida	Microbrightfield	https://www.mbfbioscience.com/neurolucida

CONTACT FOR REAGENT AND RESOURCE SHARING

Further information and requests for resources and reagents should be directed to and will be fulfilled by the Lead Contact, James F.A. Poulet (james.poulet@mdc-berlin.de).

EXPERIMENTAL MODEL AND SUBJECT DETAILS

All experimental procedures were approved by the Berlin animal ethic committee (LAGeSo) and carried out in accordance with European animal welfare law. P18-52 C57BL/6J mice of both sexes were used for dendritic stimulation experiments. For thalamic stimulation experiments, C57BL/6J (FEM Charité) and fosGFP (The Jackson Lab, Stock No 014135) mice of both sexes were used. For monosynaptic connectivity NEX-cre (Goebbels et al., 2006) x Ai9 (The Jackson Lab, Stock No 007909) mice, fosGFP mice (The Jackson Lab, Stock No 014135), and GAD-67 (Tamamaki et al., 2003) mice of both sexes were used.

METHOD DETAILS

Surgery and intrinsic optical imaging

Mice were anesthetized with 1%–2% isoflurane in O_2, then dental cement and glue were used to implant a lightweight metal post and recording chamber over primary somatosensory cortex. 30 minutes prior to surgery mice were administered a subcutaneous injection of metamizole (200 mg/kg). During anesthesia, a rectal probe and heating pad were used to maintain mouse core body temperature at 37°C. After surgery, mice were placed on a heating pad at 37°C until their recovery was complete. For 24 hours after surgery, metamizole was added to drinking water (200 mg/ml). In their home cages, mice had access to food and water *ad libitum* and were checked and weighed daily. Primary somatosensory whisker or forepaw cortex were identified with intrinsic optical imaging or stereotactic coordinates of the C2 whisker or forepaw, respectively. All anesthetized recordings were made under 1.5 g/kg urethane anesthesia. For awake experiments mice were head-restrained and paw-tethered as previously described (Milenkovic et al., 2014; Zhao et al., 2016). A force-feedback sensing arm (Aurora Scientific, Dual-Mode Lever Arm systems 300-C) was placed on the ventral surface of the tethered forepaw to monitor paw movement and allow identification of quiet, resting periods associated with slow cortical activity.

Virus injections

P8-12 mice were anesthetized using i.p. injections of a ketamine (120 mg/kg) and xylazine (10 mg/kg) mix and placed in a stereotactic frame (Angle Two, Leica). Stereotactic coordinates were determined and a craniotomy was performed by drilling over the somatosensory barrel cortex (1.3 mm posterior and 3 mm lateral to Bregma) or the forepaw cortex (0.2 anterior and 2 mm lateral to Bregma). Next, a glass injection pipette (10 μm diameter tip) containing the viral vector solution was connected to an oil piston pressure injection system (MO-10; Narishige) and inserted into layer 2/3 (100-300 μm from pial surface) through the intact dura.

Cortical neurons were infected with channelrhodopsin-2 (ChR2) using an adeno-associated viral vector (AAV2/9) containing pAAV-αCaMKII-hChR2(T159C)-p2A-EYFP or pAAV-αCaMKII-hChR2(E123T/T159C)-p2A-EYFP (Berndt et al., 2011). 500-1000 nL of virus were injected slowly at 50 nl/min. The injection pipette was removed slowly, the brain covered with petroleum jelly (Vaseline), and the skin resealed. Mice were left in their home cage for 21-40 days while waiting for ChR2-EYFP expression. To infect the ventral posteromedial nucleus (VPM) and the posteromedial nucleus (POm) of the thalamus, a lentivirus encoding ChR2-EYFP (pLenti-Synapsin-hChR2(H134R)-EYFP; Addgene 20945) was injected in P9-12 mice (Jouhanneau et al., 2014). The procedure was similar to that for cortical infection except that the craniotomy was performed at 1.8 mm posterior and 1.75 mm lateral to Bregma (VPM) or at 1.8 mm posterior and 1.25 mm lateral to Bregma (POm). An injection pipette was inserted to a vertical depth of 3.45 mm (VPM) or at 2.8 (POm). At that point, 500-600 nL of viral solution were injected slowly at a rate of 50 to 100 nL per minute. Mice were left for 2 weeks while waiting for ChR2 expression after which a second craniotomy was made over the hemisphere contralateral to the recording (1.8 mm posterior; 2 mm lateral) for the insertion of an optical fiber (200 μm diameter; Thorlabs) coupled to a 450–480 nm blue light source (473 nm DPSS Laser System; LabSpec) into the somatosensory thalamus. To optogenetically activate VPM or POm neurons, a 3 ms light pulse (~40 mW) was delivered at 0.25 Hz. In some experiments, VPM or POm projections were directly activated by

blue light pulses (3 ms, ~40 mW) delivered to the surface of the brain that lay over the recording site. Histological sections from every mouse were used to confirm the thalamic infection site and the distinctive cortical axonal projection for VPM (L5b and L4) and POm (L5a and L1).

Two-photon targeted whole-cell patch clamp recordings

To access the brain for electrophysiological recordings, the skull was covered with Ringer's solution (in mM): 135 NaCl, 5 KCl, 5 HEPES, 1.8 $CaCl_2$, 1 $MgCl_2$ and a small craniotomy (~1 mm diameter) was made over primary somatosensory cortex to expose the brain and the dura was carefully removed with a needle. For two-photon optogenetic stimulation experiments a drop of 1.8% agarose in Ringer's solution was placed on top of the craniotomy to stabilize the brain. A Femto2D *in vivo* two-photon laser-scanning microscope (Femtonics) was used to visualize cells at 920 nm, for EYFP identification or 820 nm, for Alex Fluor 594 dye (Thermo Fisher) identification with a Chameleon Ultra II (Coherent) Ti-sapphire pulsed laser light source via a 40x 0.8 NA water immersion objective (Olympus). Two high-sensitivity photomultipliers (PMT) were used to detect fluorescent signals. Imaging was controlled with MES software (Femtonics) running in MATLAB (MathWorks). Whole-cell patch clamp recordings were made with 2 mm borosilicate glass electrodes (Hilgenberg) with a resistance of 5-7 MΩ. Recording pipettes were filled with intracellular solution containing, in mM: 135 potassium D-gluconate, 4 KCl, 10 HEPES, 10 phosphocreatine, 4 MgATP, 0.3 Na3GTP (adjusted to pH 7.3 with KOH), 2mg/ml biocytin for anatomical reconstructions and Alexa Fluor® 594 dye (Thermo Fisher). In a subset of experiments, 1 mM QX-314 bromide (Tocris), or 1 mM MK-801 maleate (Tocris), or 200 μM D-890 (Abcam) were added. Recordings were made using an Axon MultiClamp 700B amplifier (Molecular Devices) in current clamp mode with an Ag/AgCl ground electrode in the recording chamber. Using motorized micromanipulators (Luigs & Neumann) the pipettes were inserted into the brain under visual control at an angle of 34° applying positive pressure of 130-180 mbar. While lowering pipettes into the tissue until about 120 μm depth, pressure was gradually reduced to 50-80 mbar. Cells were approached at low positive pressure (30 mBar) and contact with a neuron was identified by live two-photon images and the resistance changes were visualized on an oscilloscope (Tektronix TDS2024C). Upon contact, negative pressure was applied to form a gigaseal and subsequently break in and enter whole-cell recording configuration. To reduce the level of optical stimulation of ChR2-expressing neurons during the visualization of the EYFP signal, a few, low-power (~5 mW) raster scan images were collected at 920 nm then, once a neuron was identified as expressing EYFP, we used 820 nm light to target the dark shadows of cell somata against the background of the intracellular fluorescent Alexa Fluor 594 dye. Recordings were filtered at 10 kHz and digitized at 20 kHz via an ITC18 (Heka) analog-to-digital converter connected to a PC under the control of IGORpro (Wavemetrics). The membrane potential was not corrected for the liquid junction potential.

For monosynaptic connectivity experiments, up to 4 recording pipettes were inserted into the brain and 2 to 4 pyramidal neurons were targeted as previously described (Jouhanneau et al., 2015, 2018). To evoke single action potentials, square current pulses (10-20 ms, 100-400 pA) were injected into each cell at a rate of 1 or 0.5 Hz. Z stack images (2 μm/slice) were made after the termination of the recordings to confirm cell identity.

Subcellular two-photon optogenetic stimulation

Two-photon optogenetic stimulation was performed with the imaging laser source (at 920 nm wavelength) opened for 10 ms to deliver 10-25 mW (measured below objective). Somatic stimulation was performed with a spiral scan line (diameter: 8 μm, thread pitch: 0.45 μm). The spiral scan line was scanned two times with constant speed (19 μm/ms) during this stimulation epoch.

The cell was filled with red Alexa Fluor 594 during whole-cell recordings and the dendrites were imaged at 820 nm. At the beginning of each recording, at least 30 somatic stimuli were applied and the amplitude of an average V_{hyp} response was evaluated online as a measure of the neuronal responsiveness to light; the power of further subcellular stimulations could then be tuned accordingly. Next, dendritic stimulations were targeted to thin apical or basal dendrites using the red Alexa signal in the dendrites for *in vivo* guidance. Dendrites were selected with no neighboring dendrites in the same optical plane (not closer than ~15 μm). Apical dendrites were identified by following the branching of the apical dendritic trunk emerging from the top of the pyramidal cell body and moving toward the pial surface. In contrast, basal dendrites were identified by following the branching of laterally emerging dendrites moving around the soma focal plane. We then used a zigzag scan line (side length: 1 μm, displacement: 0.1 μm) to activate individual dendritic regions at the same speed as somatic stimulations, resulting in 10 epochs in 10 ms. Cells were stimulated 250 times in one trial at 3 Hz; following each trial, the stimulation positions were checked and readjusted if necessary. 3 to 6 trials were performed per dendrite. Optical stimulation was controlled using MES software (Femtonics) running in MATLAB (MathWorks).

Histology

Mice were deeply anesthetized by i.p. injection of urethane and transcardially perfused with 4% paraformaldehyde (PFA). The brain was fixed in 4% PFA overnight and stored in phosphate buffer. A Leica VT1000 S vibrating microtome was used to make 100 μm thick coronal or tangential slices that were subsequently stained for cytochrome oxidase and biocytin with a standard ABC kit (Vectastain) with DAB enhancement. Slices were mounted in Mowiol and stored at 4°C before stained neurons were reconstructed using NeuroLucida software (MicroBrightField). Any putative GABA-ergic inhibitory interneurons were excluded from the dataset.

Electrophysiological inclusion parameters

Recorded neurons were included in the dataset only when they met specific parameters related to the health of the neuron and quality of the patch. If the average V_{hyp} V_m was above −50 mV, the cell was excluded. At the beginning of each recording, a firing pattern was assessed by injecting 0.5 s steps of current (−200, −100, +50, +100, +150, +200, +250 and +300 pA). Neurons which did not respond with action potentials (APs) to the +300-pA stimulus or whose APs reached peak amplitudes below −10 mV were excluded. Only recordings with an access resistance below 60 MΩ were included in the dataset.

Compartmental model

Numerical simulations for Figure 7 used a compartmental model of one of the reconstructed layer 2/3 pyramidal neurons. The soma contours created with the Neurolucida software were replaced by a series of cylinders with the same total membrane surface area. The model used intracellular resistivity R_i = 200 Ω cm and membrane capacitance C_m = 1 μF/cm^2. Dendrites were discretized into compartments with a length of ≤ 0.1 times the frequency-dependent length constant at 100 Hz.

A leak conductance g_{leak} was distributed uniformly across soma and dendrites. Active properties consisted of a non-inactivating voltage-gated amplifying current: $I_{VGC} = \overline{g}_{VGC}\, n\, (V - E_{VGC})$ where we set the reversal potential E_{VGC} to a strongly depolarized value of 50 mV. The gating variable n evolved according to $\tau_n dn/dt = n_\infty(V) - n$. The activation function $n_\infty(V) = 1/1 + exp(-(V - V_h)/k)$ was characterized by its half activation voltage V_h and the reciprocal slope parameter k. The activation time constant τ_n of the current was considered voltage-independent. The peak conductance density $\overline{g}_{VGC}$ of the amplifying current was a parameter that was used for basal dendrite compartments further than x_b μm from the soma and for apical compartments further than x_a μm from the soma, otherwise it was set to 0.

Simulations were performed to constrain the seven undetermined parameters, which were independently varied over physiologically plausible ranges: g_{leak} (0.08-0.4 mS/cm^2), $\overline{g}_{VGC}$ (0.005-0.15 mS/cm^2), x_b (0-160 μm), x_a (0-300 μm), V_h (−57 - −39 mV), k (0.5-5 mV), τ_n (0.1-10 ms). An optogenetic stimulus was simulated as a local conductance change in a basal compartment ~70 μm from the soma (see Figure 7A) or at the soma itself. The conductance time course was described by an alpha function: $g_{OG} = \overline{g}_{OG}\, exp(-(t - \tau_{OG})/\tau_{OG})\, t/\tau_{OG}$ *for* $t > 0$, where the time constant τ_{OG} = 6 ms was fit to the experimental data in which the soma was directly stimulated and recorded. The membrane current generated by the optogenetic stimulus was $I_{OG} = g_{OG}\, (V - E_{OG})$ with reversal potential E_{OG} = 0 mV.

For each parameter combination, the conductance stimulus was applied during V_{hyp} where the uniform holding potential was −60 mV and during V_{dep} with holding potential −50 mV. The peak conductance of the optogenetic stimulus $\overline{g}_{OG}$ was varied over a range to obtain somatic depolarizations of up to 1.5 mV for the basal input (see Figures 2D and 2F) and up to 4.2 mV for the somatic input (see Figures 1G and 1I). The ratio of the somatic voltage amplitudes in V_{dep} to V_{hyp} was computed and the sum squared error with the experimental observations was computed for basal and somatic stimuli combined in order to find parameter sets that account for the amplification of the basal but not the somatic inputs. Simulations and analysis were carried out in NEURON (Hines and Carnevale, 1997) and MATLAB (the MathWorks, Inc.).

QUANTIFICATION AND STATISTICAL ANALYSIS

Datasets

Subcellular ChR2 stimulation results included data from primary whisker and primary forepaw somatosensory cortex. As we observed identical findings in both regions, the datasets were combined. All experiments using awake mice were made from primary somatosensory forepaw cortex. A subset of the VPM and POm stimulation dataset was already published (Jouhanneau et al., 2014); however, the comparison between V_{dep} and V_{hyp} response was not previously reported. Likewise, a subset of monosynaptic connections used in the analysis shown in Figure 5 was included in previous analyses (Jouhanneau et al., 2015, 2018), however, the comparison of $_u$EPSP amplitude during V_{hyp} versus V_{dep} was not previously reported.

Selection of V_{hyp}/V_{dep}

Subcellular OP, thalamic and single AP evoked responses were separated into responses during depolarized (V_{dep}) or hyperpolarized (V_{hyp}) phases based on the prestimulus V_m. Typically, a histogram of the V_m was generated and the point equidistant from the two normally distributed curves over V_{hyp} and V_{dep} states was taken as a reference to split the states. Trials falling into a ± 2 to ± 5 mV window from the divide, or those sweeps with a standard deviation > 1.5 mV (as measured between two windows −50 to −1 ms and +50 to +100 ms), were considered to be in transition states and removed from further analysis. In cases without clear bimodal distributions of the V_m, and in awake data, V_{hyp} and V_{dep} thresholds were defined at a set distance from the most hyperpolarized value in the sweep. All data were visually inspected to confirm the automatic sorting. Layer 2/3 neurons fire extremely sparsely, but those segments with spontaneously occurring APs were removed from further analysis.

Amplitude measurement of subthreshold responses

The amplitudes of optogenetic potentials (OPs), VPM responses and $_u$EPSPs were measured from the averaged response. The amplitude of the response (signal) was measured as the difference between the average V_m ± 0.5 ms around the peak response and the 1 ms average of the V_m baseline (−1 to −2 ms before stimulus onset). Noise was calculated by randomly selecting a time

point before the onset of the stimulus and measuring the V_m difference between the 1 ms average around each time point and the amplitude of the response. The signal to noise ratio was calculated by measuring the variance of response amplitude and the background V_m variance −30 to −10 ms prior to the stimulus onset on each individual trial. Next the mean variance was calculated and the response variance (signal) was divided by the background variance (noise). Any monosynaptic connectivity data with a hyperpolarizing response to the presynaptic spike, suggesting inhibitory neuron activation, were removed from the dataset. The latency was defined as the crossing point of two linear fits: the first from −15 ms to −5 ms prior to the presynaptic spike (for monosynaptic connectivity data) or onset of the laser pulse (for optogenetic stimulation data), the second between time points corresponding to 20 to 80% of the peak V_m response amplitude. In addition, we calculated the half width of the OPs as the difference in time between 50% of the rising phase and 50% of the decay phase of the evoked response. The expected OP amplitude value in V_{dep} was calculated using the change in pre-stimulus V_m and assuming a reversal potential of 0 mV for OPs.

Input resistance

−100 pA, 80 ms current pulses were injected via the recording pipette at 5.55 Hz. The V_m responses to the current pulses were then split into V_{dep} and V_{hyp} states, as discussed above, and averaged. Access resistance was subtracted offline using an exponential fit of the V_m from a 2 ms period after the start of current injection (Zhao et al., 2016). The difference in V_m between the baseline and the time point at which the fit crossed the onset time of current injection was taken as the access resistance. The input resistance was calculated from the difference in V_m between the current injection response corrected for access resistance and the prestimulus V_m. Tau was calculated from the exponential fit of the relaxation phase of the V_m from 2 ms after the end of the hyperpolarizing pulse.

In vivo data statistics

Custom written scripts in IGORpro (Wavemetrics) and MATLAB (MathWorks) were used to analyze all data. Correlations between V_{hyp} amplitude and the ratio of V_{dep}: V_{hyp} response amplitude are calculated on the $\log_{10}$ of the V_{hyp} amplitude with Pearson's linear correlation in IGORpro. Correlations between ratio of V_{dep}: V_{hyp} response amplitude and stimulation site distance from the soma were calculated using Pearson's linear correlation. The mean number of stimuli delivered in V_{dep} were: Soma anesthetized 110 ± 102, soma awake 60 ± 31, basal anesthetized 192 ± 105, basal awake 114 ± 52, apical anesthetized 219 ± 140, apical awake 106 ± 75, VPM 83 ± 60, POm 90 ± 74, $_u$EPSP 69 ± 27, basal QX-314 154 ± 93, basal MK-801 226 ± 129, basal D-890 272 ± 150. For statistical analysis, we used two-tailed non-parametric tests. Paired data were tested using the Wilcoxon signed rank test and unpaired data with the Wilcoxon rank sum test unless otherwise stated. Data in results and on figures show mean ± standard deviation (SD) unless otherwise stated.